Detection of broken rotor bars in non-linear startups of inverter-fed induction motors

V. Fernandez-Cavero, J. Pons-Llinares, *Member*, *IEEE*, O. Duque-Perez,
D. Morinigo-Sotelo, *Member*, *IEEE*

***Abstract*— Fault detection in induction motors powered by inverters operating in non-stationary regimes remains a challenge. The trajectory in the time-frequency plane of harmonics related to broken rotor bar develops very in proximity to the path described by the fundamental component. In addition, their energy is much lower than the amplitude of the first harmonic. These two characteristics make it challenging to observe them. The Dragon Transform (DT), here presented, is developed to overcome the described problem. In this paper, the DT is assessed with non-linear inverter-fed startups, where its high time and frequency resolutions facilitate the monitoring of fault harmonics even with highly adjacent trajectories to the first harmonic path.**

Index Terms—Fault detection, Induction motors, Inverters, Rotors, Time-Frequency domain analysis.

I. Introduction

INDUCTION motors (IM) are the primary source of mechanical energy in industry. Almost all motors installed in the world (90%) are of this type. These machines can operate at fixed speed when fed from the line, but this operating mode is very inefficient. Inverter motor supply makes it possible to control the speed and adapt it to the demands of the load, which results in significant savings in the energy consumed. [1,2]. The timely detection of possible failures in these machines is of great importance to the industry and a great effort has been made in the development of appropriate techniques using different variables as a basis for diagnosis such as vibration, stator current, voltage, power, magnetic flux or acoustic noise [3]. The use of the motor supply current for fault detection is favoured by the type of sensors used, which in many cases are already present for motor control. However, the use of inverters makes fault identification more difficult due to increased noise level and the generation of additional harmonics in the stator electrical current. Other particular situations can also lead to false fault identification, such as load oscillations [4], axial-cooling-air-ducts [5] or being the number of fan blades an integer multiple of the number of poles [6]. The output frequency assigned by the inverter or its control strategy affects the amplitude or energy of the fault-related frequency components [7-9]. In this paper, the case of bar breakage harmonics during a non-linear inverter-fed IM startup is analyzed. These harmonics trajectories in the time-frequency plane develop highly adjacent to the track described by the first harmonic, which makes them difficult to observe during motor startups. Hence, diagnosing faults in inverter-fed IM operating in non-stationary regimes remains challenging.

Some techniques for fault detection in transient regimes have been proposed in the technical literature using the stator current or the stray flux [10]. These tools are based on the spectral analysis of quantities related to the motor operating characteristics [11]. Wavelet-based transforms and Wigner-Ville Distributions are reported in [12-14] for fault detection, but the appearance of cross-terms and the variable resolutions in time and frequency [15] make them inadvisable for the analysis of IM powered by inverters. The simplest atom-based time-frequency technique is the Short Time Fourier Transform, but its time and frequency resolutions are not sharp enough to identify the paths described by harmonics related to broken rotor bar and distinguish them from the first harmonic [16]. In [17], the Short Time Fourier Transform was applied for fault detection in line-fed induction motors. Other atom-based techniques provide better resolution, such as the Adaptive Slope Transform (AST) [18] and the Chirplet Transform (CT) [19,20]. The accuracy of the AST is significantly better compared to other techniques, but it does not achieve to monitor the frequency components related to broken rotor bars during the startups of IM supplied by inverters. The CT achieves the observation of the fault harmonics, but only during a particular part of the inverter-fed startup. Other techniques based on the Hilbert Huang Transform (HHT) have been applied to diagnose inverter-fed IM [21,22] although HHT cannot separate the fault-related components from the first harmonic because their frequencies and mode oscillations are too similar [16][23]. The Ensemble Empirical Mode was developed to try to overcome this drawback [24,25]. In [26] is reported the combined use of

V. Fernandez Cavero was with Universidad de Valladolid, Valladolid, 47009 Spain. She is now with Universidad Europea Miguel de Cervantes, Valladolid, 47012 Spain (e-mail: vfernandez@uemc.es).

J. Pons-Llinares is with Instituto de Ingeniería Energética, Universitat Politècnica de València, 46022 València, Spain (e-mail: jpons@die.upv.es).

O. Duque-Perez is with Research Group Adire, Instituto de Tecnologías Aplicadas a la Produccción (ITAP), Universidad de Valladolid, 47009 Valladolid Spain (e-mail: oscar.duque@eii.uva.es).

D. Morinigo-Sotelo is with Research Group Adire, Instituto de Tecnologías Aplicadas a la Produccción (ITAP), Universidad de Valladolid, 47009 Valladolid Spain. He is also with Research Group HSPdigital, México (e-mail: daniel.morinigo@eii.uva.es)

the Ensemble Empirical Mode Decomposition and the Multiple Signal Classification for the observation of eccentricity harmonics during the startup in inverter-fed IM, but this proposal is not adequate for broken rotor bar harmonics. The non-uniform resampling of the stator current signal allows the fault harmonics observation but without quantification [27]. In [28], the authors propose the monitoring of the instantaneous speed during motor startups to improve detection of rotor faults. The reference [29] makes a comparative study of most of the mentioned tools applied to the detection of bar failures in linear startups in inverter-fed induction motors. It is analysed why these techniques do not manage to detect the fault and as their results are extensible to non-linear startups, this study is not repeated in this article.

The analysis of time-frequency techniques concludes that current transforms do not permit to retrieve the harmonic trajectories related to the fault during the startup of inverter-fed induction motors. Therefore, fault severity evaluation based on the quantification of the amplitude of the harmonics is also not possible. All these reasons led us to the development of a new technique presented in this paper, the Dragon Transform (DT). The excellent time-frequency resolution obtained turns the DT into the only transform in the technical literature capable of detecting and quantifying broken rotor bar frequency components during non-standard startups in induction motors powered by inverters. This novel technique achieves to represent the trajectories of the fault-related harmonics as very sharp lines and is assessed using various startup profiles, proving its capacity to monitor the trajectories of fault-related harmonics in very complex transient regimes, which is its main contribution. This paper is an extension of a paper presented at IEEE 12th International SDEMPED conference [30].

The structure of the paper is as follows: Section II explains how broken rotor bars are detected in transient regimes; in Section III, the fundamentals of the Dragon Transform are explained; Section IV contains the details of the laboratory experiments; the results are analyzed in section V, and the conclusions of this paper are in section VI.

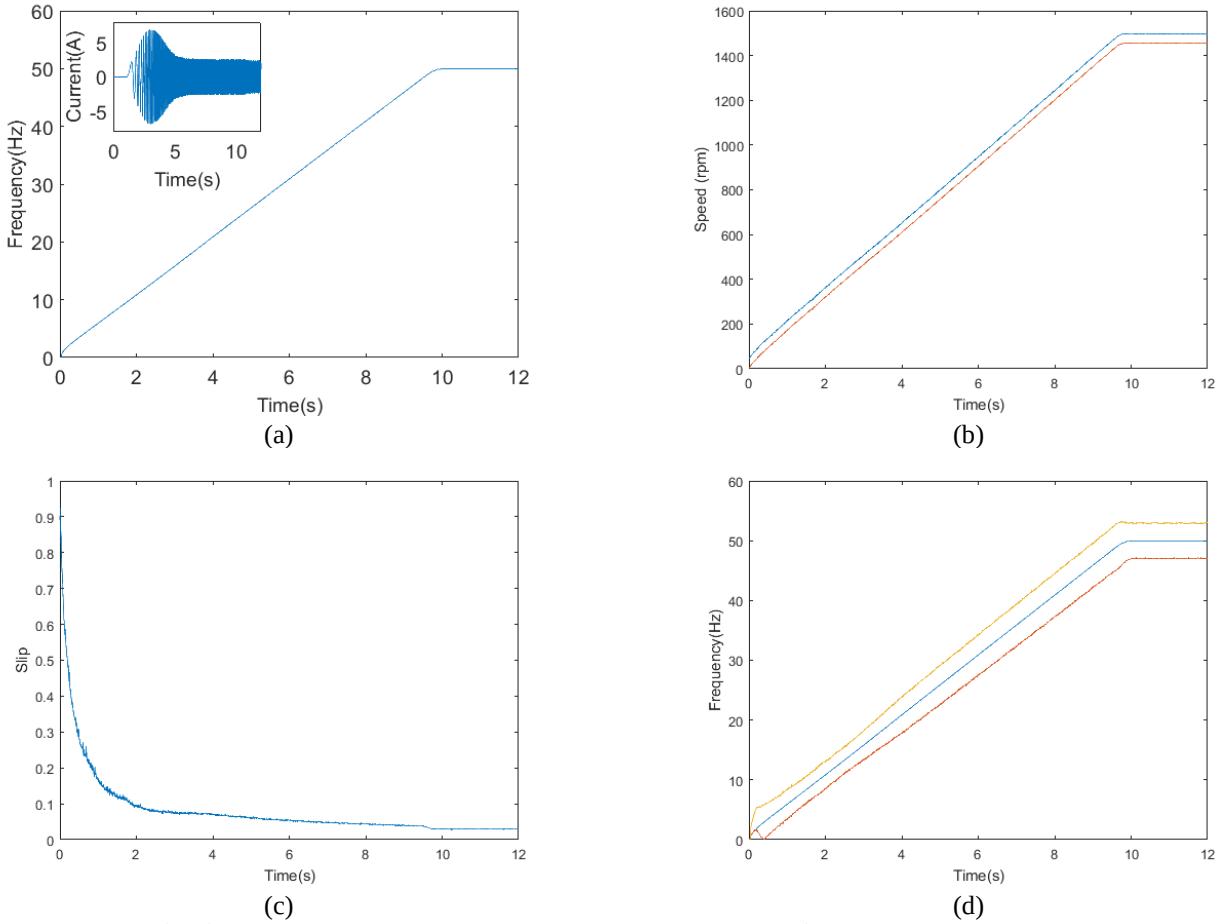

Fig. 1. Time evolution of the following magnitudes, during the startup and subsequent steady state of the induction motor with a bar breakage: (a) First harmonic and stator current; (b) Motor speed (red) and synchronous speed (blue); (c) Slip and (d) First harmonic in blue together with bar breakage components in red.

II. Detection of Broken Rotor Bars in Transient Regimes

An inverter permits the user to set the starting length and the trajectory or time evolution of the main frequency of the voltage. The output voltage frequency will increase from zero to the final operating value following a certain profile in time whose shape will depend on the real application. In Fig. 1(a) it is shown the trajectory in the time-frequency plane of the main frequency or fundamental component of an inverter-fed motor following a linear startup, which increases from 0 to 50 Hz in ten seconds. The stator current is also shown in the top left

corner. Fig. 1(b) shows the profile of the synchronous speed during the startup as a result of the profile shown in Fig. 1(a). The motor speed (in red) follows a parallel profile but behind the synchronous speed. As these speeds are very close, the slip is very low, as it is observed in Fig. 1(c). The slip (*s*) is calculated as follows:

$$s = \frac{n_1 - n}{n_1} \quad (1)$$

where n_1 is the synchronous speed and n is the motor speed.

Broken rotor bars produce an unbalance of the electromagnetic field in the airgap of an induction motor. This unbalance is translated into the stator current as frequency components, giving rise to sidebands around the fundamental frequency whose values (f_{brb}) are given by:

$$f_{brb} = (1 + 2sk) f_{FC} \quad (2)$$

where s is the slip and f_{FC} is the fundamental frequency of the supply voltage (k usually equals ± 1). Therefore, when there is a fault, two harmonics or sidebands will appear around the first component. One fault-related harmonic will be above the first harmonic and the other will be below it. Both are separated from the first harmonic by $2sf_s$ Hz. During a transient, these harmonics will describe a trajectory in the time-frequency plane. The theoretical trajectories of the fundamental component and the fault-related harmonics, given by (2), are shown in Fig.1(d) for the described startup transient. As a result of the low value of the slip, these harmonic components, whose energy is very low compared to the energy of the first harmonic, evolve during the startup parallel to the main frequency. They are especially close to the first harmonic during the startup transient, making their detection particularly challenging.

In summary, the slip is very low during the startup of an inverter-fed induction motor, and therefore fault components are highly adjacent to the first harmonic and with much less energy, making it very difficult their detection. Therefore, no time-frequency technique has sufficient resolution to observe these harmonics.

III. Non Linear Evolutions Analysed through Dragon Transform

As seen in section II, the detection of the broken rotor bar harmonics during an inverter-fed startup is challenging since their trajectories in the time-frequency plane develop too close to the path described by the first harmonic. Therefore, a time-frequency transform capable of tracing them as very thin lines is necessary. Only three transforms bring good results for inverter-fed startups with linear evolutions:

- AST: enables to follow the FC evolution during the whole transient, while the bar breakage harmonics are only detected once the steady state is reached [29].
- CT: enables to distinguish the FC and bar breakage harmonics through the startup, but not during the steady state [29].
- Dragon Transform: enables to distinguish both the FC and bar breakage harmonics, not only during the startup, but also through the steady state [31].

The difficulty highly increases when dealing with non-linear startups, as with S-curve and U-curve ramps. In this case, the frequencies of the harmonics to be detected do not evolve linearly with time, describing S and U patterns, as shown in the results section (see Fig. 5). For these cases, the evolutions are not only very close, but they are much less parallel than in the linear case. Therefore, neither the AST nor the CT are suited for the analysis of inverter-fed non-linear startups. Particularly, the CT, which succeed with the linear startup, is able to follow harmonics evolving very close in the t-f plane, but only as long as their frequency changes linearly with time, which is not the case of non-linear startups.

Let us see how the Dragon Transform can adapt its atoms to fit the complex evolutions that arise in a non-linear startup. To start with, let us see the atom used. Any window could be proposed, but the Gaussian window (used in the well known Gabor transform [32]) has the best t-f energy concentration. This window might be defined as:

$$g(t) = C_\sigma e^{-\frac{t^2}{2\sigma^2}} \quad (3)$$

where $\sigma \in \mathbb{R}$ represents the parameter of dispersion or deviation and C_σ is the normalization constant, which is defined as:

$$C_\sigma = \frac{1}{\sqrt[4]{\pi}\sqrt{\sigma}} \quad (4)$$

In order to build a dragon atom, first thing is to choose a high enough deviation parameter. That way, the atom highly spreads its energy in time. For instance, the energy distribution of such a dragon atom is shown in Fig. 2 (b) circled in orange (the rest are also dragon atoms, but let us discuss that later).

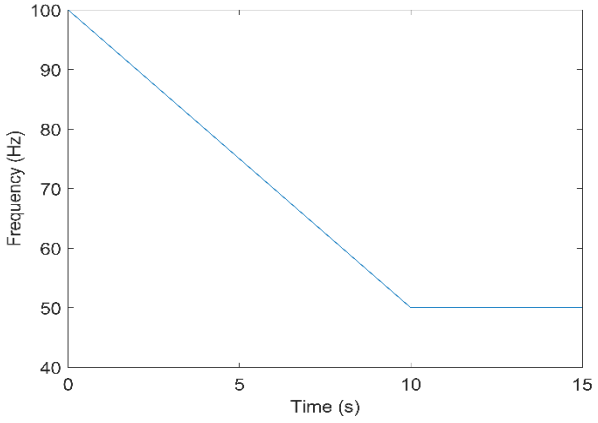

(a)

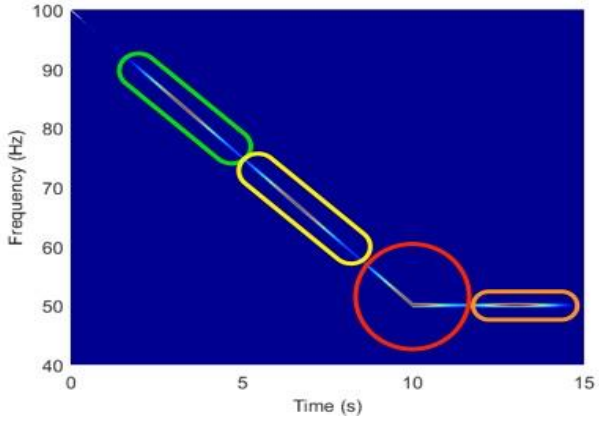

(b)

Fig. 2. (a) Trajectory in the t-f plane of monocomponent synthetic signal; (b)Energy distribution of the family dragon atoms defined to capture that trajectory.

As it can be seen, the energy is distributed forming a completely plane atom with a big dispersion in time (from 12 to 14.5 seconds aproximatelly), while its energy is well concentrated in frequency (in 50 Hz).

Then, next step is to change the point of the t-f plane where the atom is located, and more important, change the shape of that plane atom so it fits any harmonic evolution that must be detected, even those appearing in non-linear startups. Let us see with a simple example what must be obtained. Fig. 2(a) shows the trajectory of the frequency of a synthetic signal in the time-frequency plane. This frequency descends from 100 Hz to 50 Hz in ten seconds and then remains at this value for five seconds more. To analyse that signal, Dragon Transform constructs atoms whose energy distributions in the t-f plane fit that harmonic t-f evolution. Figure 2(b) shows 4 dragon atoms calculated to capture the trajectory previously described. Two atoms (enclosed in green and yellow) are generated following the descending path (transient regime). Another atom (circled in red) adapts its shape to capture the elbow of the trajectory correctly. The last atom (surrounded in orange) is for the stationary end. These atoms follow the evolution in time of the harmonic precisely. So, the dispersion of the energy of each of the four atoms occurs in the direction of the evolution of the component.

How is this achieved? Usually, to construct a normal atom, the window is multiplicated by a complex exponential as follows:

$$\Psi(t) = g(t)e^{i2\pi f_c t} \tag{5}$$

This way, since the window has a 0 Hz frequency, the central frequency of the atom is f_c. Instead of moving the atom up and down in the frequency domain, to center it at different frequencies f_c, there is a need to move each slice of the atom, at each time instant, to a different frequency, so it adapts to the evolution to be captured. To do so, instead of $f_c t$, an arbitrary angle $\theta(t)$ is used as follows:

$$\Psi(t) = C_\sigma e^{-\frac{t^2}{2\sigma^2}} e^{i2\pi\theta(t)} \tag{6}$$

In a normal atom-based transform, the derivative of that angle is f_c; therefore, the atom is centered at that frequency. In the Dragon Transform, the derivative of that angle changes with time following the evolution of the component to be detected. In other words, $d\theta(t)/dt$ is equal, at each time instant, to the harmonic frequency to be detected. For instance, for the dragon atoms circled in green and yellow in Fig. 2 (a), the time derivatives of $\theta(t)$ follow the linear evolutions of the harmonic descending from 100 to 50 Hz. In the case of the atom circled in red in that same figure, its time derivative is at first equal to that previous linear evolution, and changes to a constant value of 50 Hz when the harmonic to be detected describes a horizontal t-f evolution. The time derivative of $\theta(t)$ for the last atom circled in orange is the same for every time instant, and equal to 50 Hz.

Once the angle of the complex exponential is defined, such that its derivative is equal to the frequency of the component to be detected, the transform is obtained by correlating the atom with the signal h to be analysed:

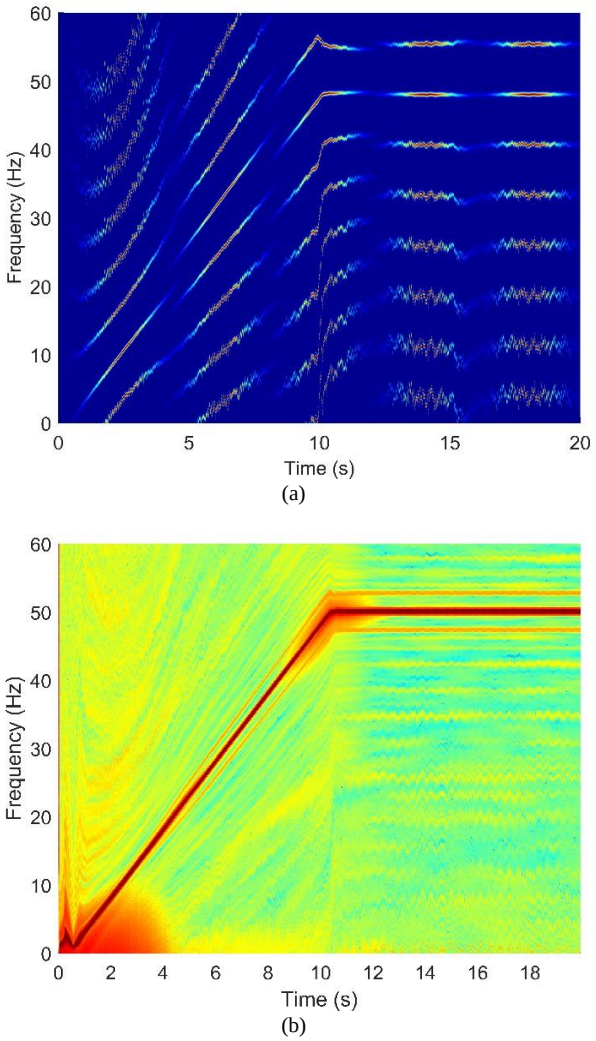

Fig. 3. Family of dragon atoms used to perform the analisys of the current of a linear startup of an inverter-fed induction motor with a broken rotor bar as shown in Fig. 1. (a) Dragon Transform result (b) [31].

$$\langle h, \Psi \rangle = \int_{-\infty}^{+\infty} h(t)\Psi^*(t)dt \tag{7}$$

The correlation of an atom centered in a point of the t-f plane with the signal provides the energy of that signal at that point (more precisely, a measure of the signal energy in the area where the atom has its energy concentrated). A general rule for this type of transform is that the energy of the harmonic to be detected has a dispersion in the t-f plane equal to the t-f dispersion of the atoms used around the harmonic evolution. In this transform, the atoms shape in the t-f plane adapts to the path of the harmonic to be detected. Therefore, since the dispersion of the atom happens along the trajectory of the harmonic to be detected, the dispersion of that same harmonic happens along its own evolution. As a consequence, the harmonic is traced in the transform t-f result as a very thin line. This enables that the evolutions of harmonics that are so closed to each other, can be depicted very precisely, even if their evolution do not follow linear paths, as the ones shown in the results section.

Let us give a detailed mathematical description of the Dragon Transform application. First, σ is fixed to a high enough value in order to obtain a flat atom. Taking $\sigma = 3.9894$ the atom

covers almost 3 seconds in time (atom circled in orange in Fig. 2(b)). Since industrial startups might last even 60 s, with this longer signals flatter atoms might be used. Then, a matrix of points through the t-f plane is defined, through a set of instants (one for each current sample) and a set of frequencies covering the bandwidth where the fault harmonics evolve (e.g., 200 frequencies covering from 0 to 65 Hz). As a previous step, the FC evolution $f_{FC}(t)$ is obtained through the current [18]. The speed is measured or estimated, to determine the slip $s(t)$, e.g. taking profit of the speed estimator used in the control scheme.

Next, the evolutions to be detected are determined. In the case of bar breakage detection, assigning different values of k in (2), a family of parallel evolutions covering the whole t-f plane is obtained. That way, no matter which point (t_c, f_c) is analysed, only one evolution of that family crosses that point, defining the dragon atom to be used, which would be perfectly adapted to that evolution. For instance, taking $k = 0$, the FC evolution is obtained, while $k = \pm 1$ are the values to obtain the bar breakage harmonics.

From here, the following procedure is followed for every point (t_c, f_c) to be analysed: the value of k that defines the evolution of the harmonic crossing that point is calculated (8), the instantaneous frequency of the evolution is obtained (9), being integrated to obtain the instantaneous angle of the complex exponential in the t-f atom, and finally the atom is constructed (10) and the correlation is obtained.

$$k(t_c, f_c) = \frac{1}{2s(t_c)}\left[\frac{f_c}{f_{FC}(t_c)} - 1\right] \quad (8)$$

$$f(t) = \big(1 + 2k(t_c, f_c)s(t)\big)f_{FC}(t) \rightarrow \theta(t) = \int f(t)dt \quad (9)$$

$$\Psi(t) = C_\sigma e^{-\frac{(t-t_c)^2}{2\sigma^2}} e^{i2\pi\theta(t)} \rightarrow \langle h, \Psi \rangle \quad (10)$$

Let us see an example with a quasi linear evolution of the harmonics (more complex non-linear startups are presented in the results section). The example analysed is the current shown in Fig. 1 (a): the startup current of an inverter-fed induction motor with a broken rotor bar. As explained in section II, there are three harmonics in that signal that need to be detected, which are plotted in Fig. 1 (d). The energy distributions of the atoms family constructed are shown in Fig. 3(a). Finally, Fig. 3(b) shows the Dragon Transform result of the correlation of the signal with this family of dragon atoms; showing the complete evolutions of the FC and the bar breakage harmonics.

IV. The Laboratory Setup

The test bench used in this work was described in [27] where a picture of it is shown. An induction motor with the following specifications was used: rated power of 1.1 kW; star connection; 400 V rated voltage; 1410 rpm rated speed, 7.4 Nm rated torque, and 2.6 A rated current. It was loaded with a Lucas Nülle powder magnetic brake, which also incorporates a torque and speed meter.

Data was collected using a National Instruments cDAQ-9174 chassis with an NI-9215 module. Two Hall effect sensors by LEM were used as current (LA 25-NP) and voltage (LV 25-P) transducers. The sampling rate was 60 kHz and the DAQ has a built-in antialias filter at 30 kHz. The acquired signal is digitally filtered using a low-pass filter with a cut-off frequency of 128 Hz. Then the data was decimated to a sampling rate of 256 Hz, for a 128 Hz bandwidth using the technique presented in [33].

The motor was tested at two load levels and two conditions: healthy state and full broken rotor bar, which was simulated by drilling a hole in the junction of a bar with the cage end ring. The lowest loads were between 2.2 and 3.0 Nm, corresponding to 29 to 40% of the motor rated load. The higher loads were between 3.6 and 4.0 Nm that correspond to 48 to 54% of the nominal motor torque.

Two inverters were used as motor supply (PowerFlex 40 by Allen Bradley, and Altivar 66 by Telemecanique) with a scalar open-loop control strategy so as not to affect the amplitude of fault-related harmonics. In any case, according to [6], the use of close-loop speed controllers should have not affected the tracking of fault-related trajectories in the time-frequency plane. These inverters allow the user full control of the startup transient. The supply voltage amplitude and its frequency increase from zero to the final cruise values configured by the user. By default, this increment follows a linear profile over time, but some inverters offer the functionality of following a different one: an S or U curve. The first is used in elevator applications to provide passenger comfort, and the second in valve actuation to prevent water hammer. In this work, the inverters were configured to start the motor following 10 second long S and U profiles with a final frequency of 50 Hz. The voltage was collected to calculate the fundamental frequency and the synchronous speed over time, as explained in [18]. The speed was also measured for the calculation of the motor slip. This information permits the computation of the fundamental component and fault-related harmonics trajectories in the time-frequency plane, which are necessary to apply the Dragon Transform to the stator current and compute the spectrogram.

V. Results

The proposed technique has been validated under different conditions in an extended number of tests; the motor load level was also changed. In some tests, the load torque was low and in other tests was higher. In this section, two fault severity levels are shown (healthy and full broken rotor bar). In the case of the Allen Bradley inverter, the motor operating under low load level will be shown, while the Telemecanique inverter is used to illustrate the case of the motor operating under high load level.

Two types of startup are shown; Fig. 4 (a) corresponds to an S-shaped startup with the Allen-Bradley inverter and Fig. 4 (b) to a U-shaped one with the Telemecanique inverter. It can also be seen in these figures a detail of the current consumed by the induction motor in two of the laboratory experiments. The theoretical trajectories of the fault-related harmonics are also depicted and it is seen that they evolve very close to the fundamental component in the time-frequency plane.

Fig. 5 shows the result of the analysis of the startup currents with the Dragon Transform. In this case, the motor is fed by the Allen-Bradley inverter following an S-curve startup ramp. In Fig 5 (a) the case of a motor in healthy condition is shown. Figs. 5 (b), (c) and (d) show the case of the same motor with one

broken rotor bar. Three details illustrate separately the evolutions of the fault-related harmonics at the beginning, middle and end of the startup. As it can be observed, the time-frequency atoms generated by the Dragon Transform are thin enough providing a sharp time and frequency resolution that achieves to capture the energy of the fault-related harmonics and differentiate it from the energy of the first harmonic, even during the initial slope of the startup, where they are closer to the main component. The adaptation of the atoms to the trajectory of the main component in the time-frequency plane is also remarkable. The atoms achieve to represent smoothly the S-shape profile programmed with the inverter.

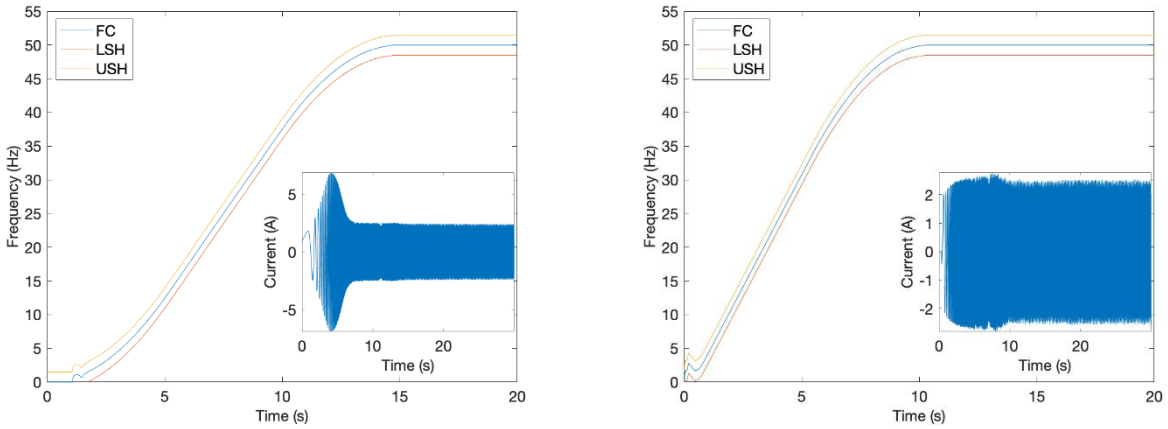

Fig. 4. Theoretical trajectories in the time-frequency plane of the fundamental component and broken rotor bar related harmonics in an inverter-fed induction motor: (a) S-curve startup ramp and stator current of the inverter-fed IM powered by Allen Bradley Power Flex 40 inverter; (b) U-curve startup ramp and stator current of the inverter-fed IM powered by Telemecanique Altivar 66 inverter.

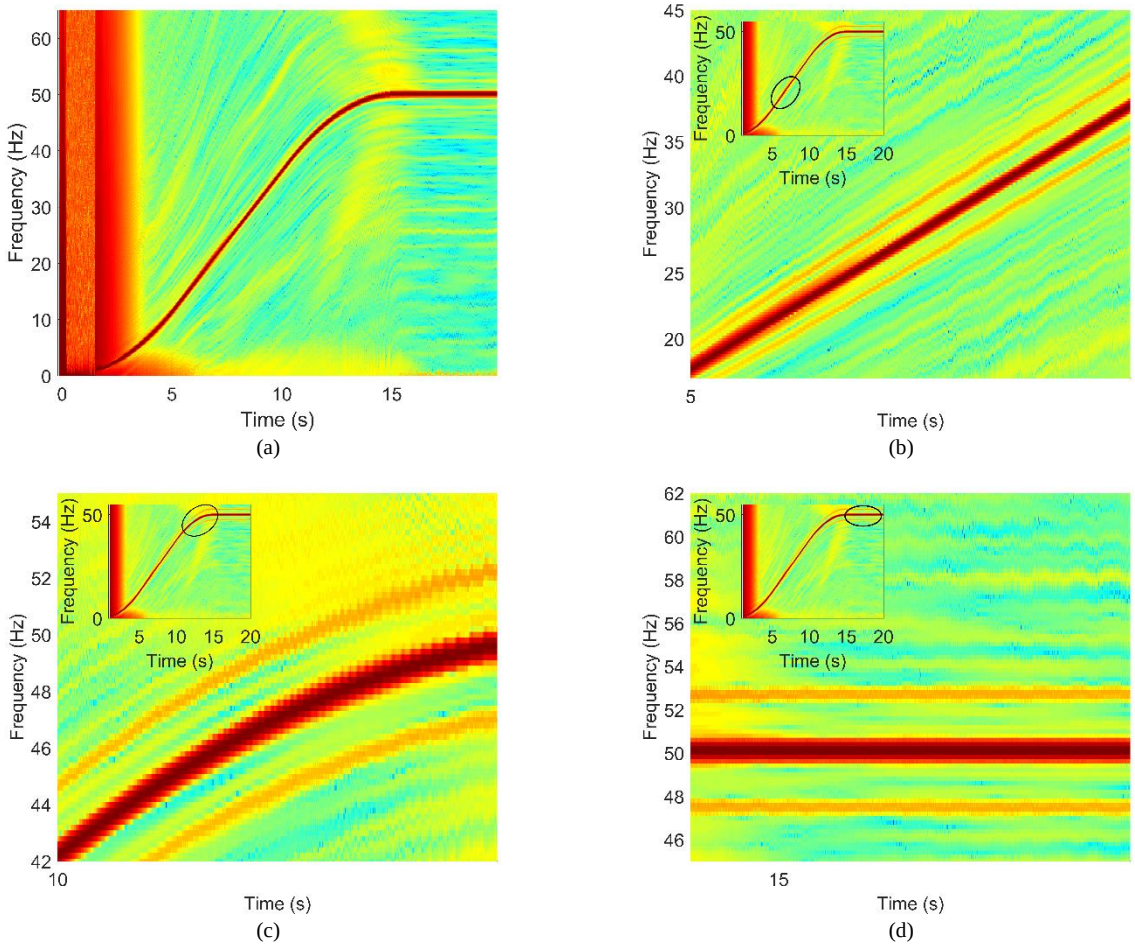

Fig. 5. Spectrograms of the stator current of an IM powered by an Allen Bradley inverter with a S-start up and low motor load; (a) Healthy Motor; (b) Motor with one broken rotor bar and zoom of the intial ramp of the transient regime; (c) Motor with one broken rotor bar and zoom of the final startup transient; (d) Motor with one broken rotor bar and zoom of the final steady state operation.

Fig. 6 shows the result for the motor fed by the Telemecanique inverter programmed with a U-shaped startup ramp, respectively. This figure confirms the previous results. In this case, even though the slope of the initial ramp is higher than in the previous case, the time-frequency atoms generated are again thin enough and adapt efficiently to this kind of trajectory, achieving an excellent detection of the fault-related harmonics, even at the first moments of the startup where a sudden change in the trajectory of the first harmonic happens.

The quantification method presented permits to obtain the time evolution of the harmonics amplitudes through the whole startup transient and subsequent steady state operation.

The quantification results for the U-start up case are shown in Fig. 7 (similar results are obtained for the S-start up). This figure includes the quantification for the same motor, startup profile, load and healthy condition. This quantification is the time evolution of the energy density along the trajectories of the bar breakage harmonics. Differences between the trajectories and energies for the two conditions states are clearly observable. Therefore, this quantification techniques can be used for fault detection during an inverter-controlled IM startup.

Finally, it must be mentioned that, even if the Dragon Transform is a very powerful technique, it has limitations. As it can be observed in the lower left corner of Fig. 5 (a) and Fig. 6 (a), there is an increase of energy not related to any evolution of the harmonics. This is called the border effect, and appears in every atom-based t-f transform. It appears on the zones of the t-f plane where the atoms centered have some of their evolutions outside the time interval where the current has been captured. In those points, the correlation defined in (7) cannot be properly calculated, since for a certain interval of the t-f atom, there is no current to correlate with. This causes an artificial energy increase in that zone. The shape of that border effect depends on the shape of the atoms used (left lower corner in this case). If the startup is too fast, the evolutions of the harmonics may take place more and more in that zone, and are covered. For instance, Fig. 8 shows faster S-startups (4 s (a) and 3 s). It can be seen how the distinction is more complicated, and only the last part of the startup evolutions can be clearly observed. Nevertheless, it must be mentioned that industry applications usually use inverter-fed induction motors to softly reach a certain operation point, not usually programing such fast startups (e.g., 60 s is a typical startup time for deep well motor pumps). In the case of electric vehicles, startups as fast as the one shown in Fig. 8 might take place, but in this case synchronous motors are preffered, which is also the case of industry applications with fast varying speeds.

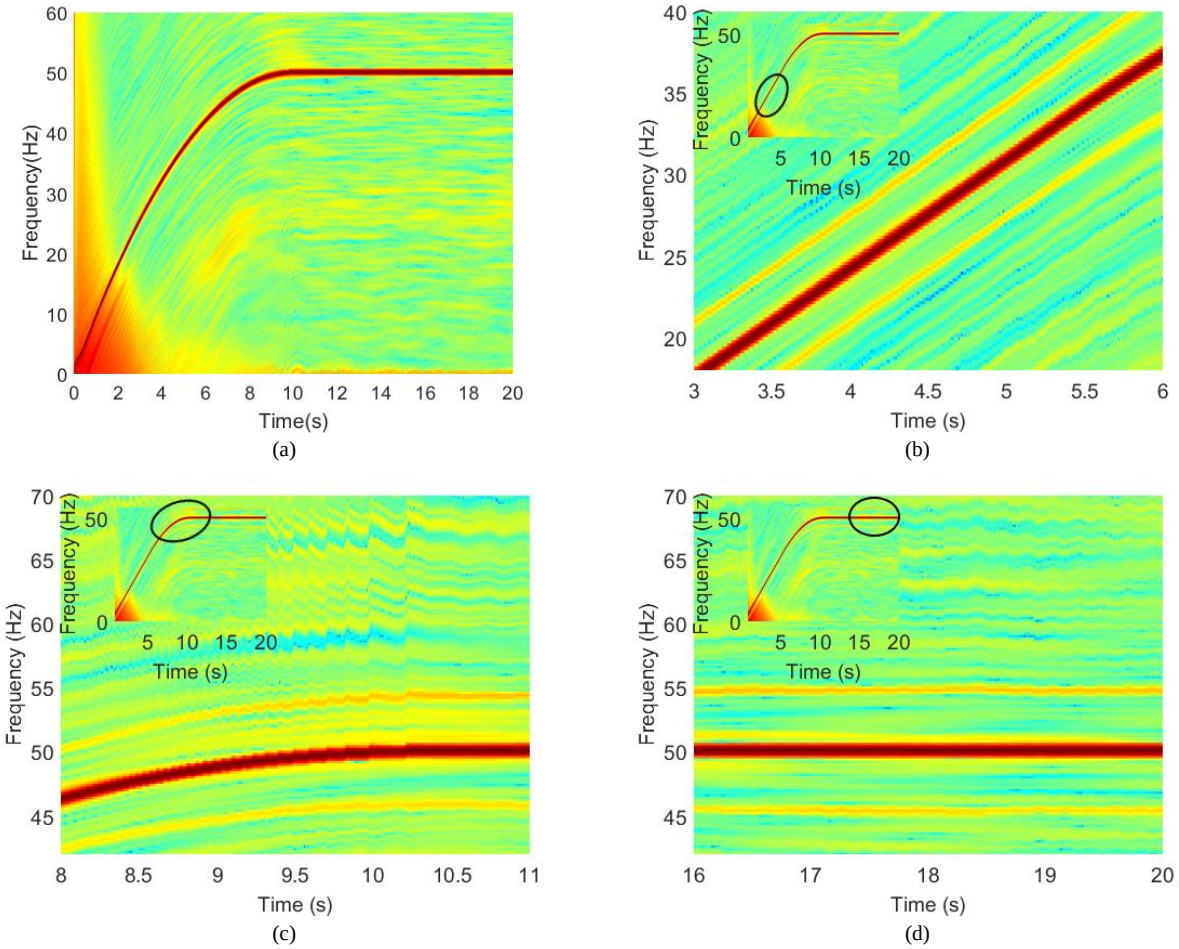

Fig. 6. Spectrograms of the stator current of an IM powered by a Telemecanique inverter with a U-start up and low motor load; (a) Healthy Motor; (b) Motor with one broken rotor bar and zoom of the intial ramp of the transient regime; (c) Motor with one broken rotor bar and zoom of the final startup transient; (d) Motor with one broken rotor bar and zoom of the final steady state operation.

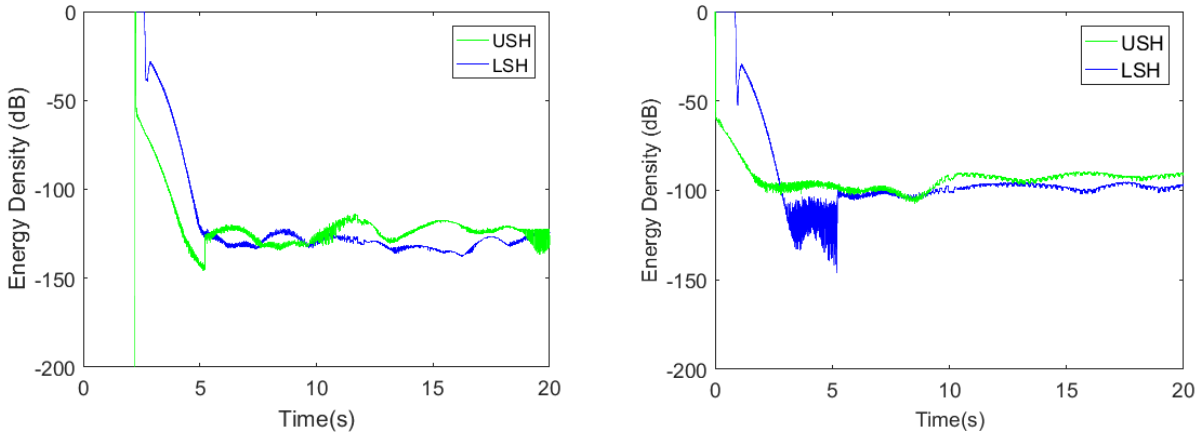

Fig. 7. Quantification curves of the fault severity during the startup transient. IM powered by an Telemecanique inverter (TM) following a U-start up and medium load: (a) Healthy condition; (b) One broken rotor bar.

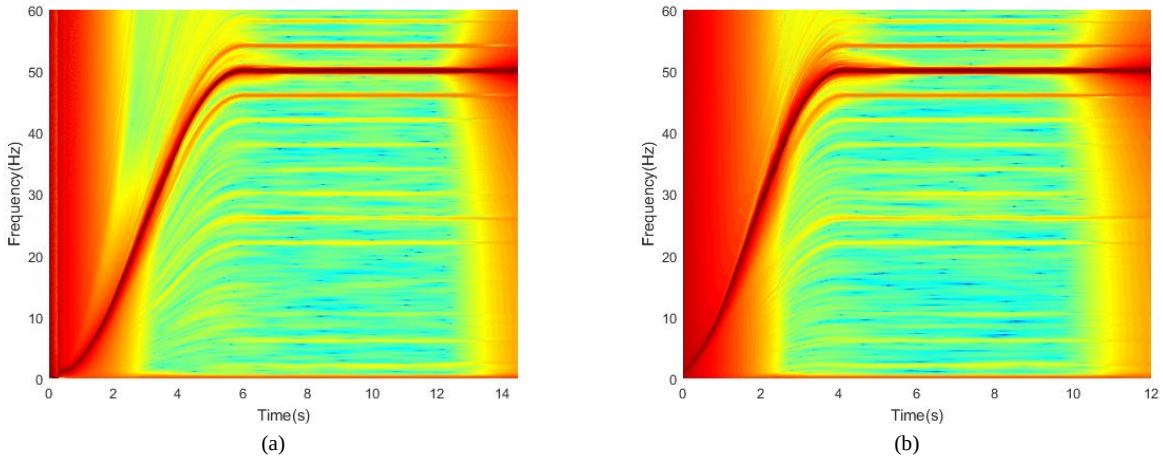

Fig. 8. Faster S startups: 4 seconds (a) and 3 seconds (b).

VI. Conclusions

The use of inverters to supply IM is widespread in many industry and service applications such as elevators, pumping, and traction. The power converter allows precise control of the IM startup profile over time. It permits setting the startup duration and the frequency-time profile, which is adequate for some applications such as lifting and pumping. During the startup transient, the trajectories of frequency components related to bar breakages develop much in the vicinity of the first harmonic path. Tools for time-frequency analysis, such as the Short-time Fourier Transform, do not achieve good enough time and frequency resolutions to identify those fault-related harmonics from the main one. This shortcoming is overcome by the proposed Dragon atoms, which adapt entirely to the shape of the theoretical trajectories of these frequency components. Therefore, their detection and severity quantification is accomplished even in low-slip operating conditions.

References

[1] J. Tolvanen, "Saving energy with variable speed drives," *World Pumps*, vol. 501, pp. 32–33, June 2008.

[2] C.M.F.S. Reza, M.D. Islam, and S. Mekhilef, "A review of reliable and energy efficient direct torque controlled induction motor drives," *Renewable and Sustainable Energy Reviews*, vol. 37, pp. 919–932, 2014.

[3] L. Frosini, "Monitoring and Diagnostics of Electrical Machines and Drives: a State of the Art", in *Proc. of 2019 IEEE Workshop on Electrical Machines Design, Control and Diagnosis (WEMDCD)*, Apr. 2019, pp. 169–176.

[4] Y. Park, C. Yang, J. Kim, H. Kim, S. B. Lee, K. N. Gyftakis, et al., "Stray Flux Monitoring for Reliable Detection of Rotor Faults under the Influence of Rotor Axial Air Ducts", *IEEE Trans. Ind. Electr.*, vol. 66, no. 10, pp. 7561–7570, 2019.

[5] C. H. De Angelo, G. R. Bossio, and G. O. Garcia, "Discriminating broken rotor bar from oscillating load effects using the instantaneous active and reactive powers", *IET Elec. Pow. Appl.*, vol. 4, no. 4, pp. 281–290, 2010.

[6] Y. Park, M. Jeong, S. B. Lee, J. A. Antonino-Daviu, and M. Teska, "Influence of Blade Pass Frequency Vibrations on MCSA-Based Rotor Fault Detection of Induction Motors", *IEEE Trans. Ind. Appl.*, vol. 53, no. 3, pp. 2049–2058, 2017.

[7] WS. Abu-Elhaija, V. Ghorbanian, J. Faiz and B.M. Ebrahimi, "Impact of closed-loop control on behavior of inverter-fed induction motors with rotor broken-bars fault," in *Proc. of 2012 IEEE International Conference on Power Electronics, Drives and Energy Systems (PEDES)*, Dec. 2012, pp. 1–4.

[8] J. Faiz, V. Ghorbanian, and B.M. Ebrahimi, "A survey on condition monitoring and fault diagnosis in line-start and inverter-fed broken bar induction motors," in *Proc. of 2012 IEEE International Conference on Power Electronics, Drives and Energy Systems (PEDES)*, Dec. 2012, pp. 1–5.

[9] M. Riera-Guasp et al, "Diagnosis of induction machines under non-stationary conditions: Concepts and tools," in *Proc. of 2013 IEEE*

Workshop o Electrical Machines Design Control and Diagnosis (WEMDCD), March 2013, pp. 220–231.
[10] J. Antonino-Daviu, "Electrical Monitoring under Transient Conditions: A New Paradigm in Electric Motors Predictive Maintenance", *Applied Sciences*, vol. 10, no. 17, 6137, 2020.
[11] V. Ghorbanian, and J. Faiz, "A survey on time and frequency characteristics of induction motors with broken rotor bars in line-start and inverter-fed modes," *Mech. Syst. Signal Process.*, vol. 54–55, pp. 427-456, March 2015.
[12] K. Teotrakool, M.J. Devaney, and L. Eren, "Adjustable-Speed Drive Bearing-Fault Detection Via Wavelet Packet Decomposition," *IEEE Trans. Instrum. Meas.*, vol. 58, no. 8, pp. 2747–2754, Aug. 2009.
[13] V. Climente-Alarcon, J. Antonino-Daviu, M. Riera-Guasp and M. Vlcek, "Induction Motor Diagnosis by Advanced Notch FIR Filters and the Wigner–Ville Distribution," *IEEE Trans. Ind. Electr.*, vol. 61, no. 8, pp. 4217–4227, Aug. 2014.
[14] T. Ishikawa, "Failure Diagnosis of Squirrel-Cage Induction Motor with Broken Rotor Bars and End Rings," in *Induction Motors - Applications, Control and Fault Diagnostics*, R. Gregor, Ed. IntechOpen, 2015.
[15] F. Hlawatsch and F. Auger, Eds., *Time-Frequency Analysis: Concepts and Methods*. London, U.K.: ISTE, 2008.
[16] J. R. Millan-Almaraza, R. J. Romero-Troncoso, R. A. Osornio-Rios, and A. Garcia-Perez, "Wavelet-based Methodology for Broken Bar Detection in Induction Motors with Variable-speed Drive," *Electric Power Components and Systems*, vol. 39, no. 3, pp. 271–287, Feb. 2011.
[17] J. Cusidó, L. Romeral, J. A. Ortega, J. A. Rosero, and A. G. Espinosa, "Fault detection in induction machines using power spectral density in wavelet decomposition," *IEEE Trans. Ind. Electron.*, vol. 55, no. 2, pp. 633–643, Feb. 2008.
[18] J. Pons-Llinares, J. Antonino-Daviu, J. Roger-Folch, D. Morinigo-Sotelo, and O. Duque-Pérez, "Mixed eccentricity diagnosis in inverter-fed induction motors via the adaptive slope transform of transient stator currents," *Mech. Syst. Signal Process.*, vol. 48, no. 1–2, pp. 423-435, Oct. 2014.
[19] S. Mann, and S. Haykin, "The Chirplet transform: A generalization of Gabor's logon transform," in *Proc. of Vision Interface*, June 1991, pp. 205–212.
[20] J. Pons-Llinares, D. Morinigo-Sotelo, O. Duque-Perez, J. Antonino-Daviu, and M. Perez-Alonso, "Transient detection of close components through the chirplet transform: Rotor faults in inverter-fed induction motors," in *Proc. of 40th Annual Conference of the IEEE Industrial Electronics Society, Feb. 2014*, pp. 3386–3392.
[21] J. Faiz, V. Ghorbanian, and B. M. Ebrahimi, "EMD-based analysis of industrial induction motors with broken rotor bars for identification of operating point at different supply modes," *IEEE Trans. Ind. Informat.*, vol. 10, no. 2, pp. 957–966, May 2014.
[22] J. Faiz, V. Ghorbanian, and B. M. Ebrahimi, "A new criterion for rotor broken bar fault diagnosis in line-start and inverter-fed induction motors using Hilbert_Huang transform," in *Proc. IEEE Int. Conf. Power Electron., Drives Energy Syst. (PEDES)*, Dec. 2012, pp. 1–6.
[23] J. A. Antonino-Daviu, M. Riera-Guasp, M. Pineda-Sanchez, and R. B. Pérez, "A critical comparison between DWT and Hilbert-Huang based methods for the diagnosis of rotor bar failures in induction machines," *IEEE Trans. Ind. Appl.*, vol. 45, no. 5, pp. 1794–1804, Sep./Oct. 2009.
[24] M. E. Torres, M. A. Colominas, G. Schlotthauer, and P. Flandrin, "A complete ensemble empirical mode decomposition with adaptive noise, " in *Proc. IEEE Int. Conf. Acoust., Speech Signal Process.*, May 2011, pp. 4144–4147.
[25] Z. Wu, and N. E. Huang, "Ensemble empirical mode decomposition: A noise-assisted data analysis method, " *Adv. Adapt. Data Anal.*, vol. 1, no. 1, pp. 1–41, 2009.
[26] R.J. Romero-Troncoso, A. Garcia-Perez, D. Morinigo-Sotelo, O. Duque-Perez, R.A. Osornio-Rios, and M.A. Ibarra-Manzano, "Rotor unbalance and broken rotor bar detection in inverter-fed induction motors at start-up and steady-state regimes by high-resolution spectral analysis", *Electric Power Systems Research*, vol. 133, pp. 142–148, Apr. 2016.
[27] T.A. Garcia-Calva, D. Morinigo-Sotelo, and R.J. Romero-Troncoso, "Non-Uniform Time Resampling for Diagnosing Broken Rotor Bars in Inverter-Fed Induction Motors," *IEEE Transactions on Industrial Electronics*, vol. 64, no. 3, pp. 2306–2315, Mar. 2017.
[28] T. A. Garcia-Calva, D. Morinigo-Sotelo, A. Garcia-Perez, and R. de J. Romero-Troncoso, "Rotor Fault Detection in Inverter-Fed Induction Motors Using Speed Analysis of Startup Transient," in *Proc. of IEEE 12th International Symposium on Diagnostics for Electrical Machines, Power Electronics and Drives (SDEMPED)*, Aug. 2019, pp. 297–302.
[29] V. Fernandez-Cavero, D. Morinigo-Sotelo, O. Duque-Perez, and J. Pons-Llinares, "A Comparison of Techniques for Fault Detection in Inverter-Fed Induction Motors in Transient Regime," *IEEE Access*, vol. 5, pp. 8048–8063, 2017.
[30] V. Fernandez-Cavero, J. Pons-Llinares, O. Duque-Perez, D. Morinigo-Sotelo, "Detection of broken rotor bars in non-linear startups of inverter-fed induction motors," in *Proc. of IEEE 12th International Symposium on Diagnostics for Electrical Machines, Power Electronics and Drives (SDEMPED)*, Aug. 2019, pp. 309–315.
[31] V. Fernandez-Cavero, J. Pons-Llinares, O. Duque-Perez, D. Morinigo-Sotelo, "Detection and quantification of bar breakage harmonics evolutions in inverter-fed motors through the dragon transform," *ISA Transactions*, vol. 109, pp. 352–367, March 2021.
[32] D. Gabor, "Theory of communication", *Journal of the IEE – Part III: Radio and Communication Engineering*, vol. 93, no. 26, pp. 429–457, Nov. 1946.
[33] R. de Jesus Romero-Troncoso, "Multirate Signal Processing to Improve FFT-Based Analysis for Detecting Faults in Induction Motors," *IEEE Trans. Industr. Inform.*, vol. 13, no. 3, pp. 1291–1300, June 2017.

V. Fernandez-Cavero received the B.S. degree in Industrial Organization Engineering and Electrical Engineering from the ICAI, Comillas Pontifical University (UPCO), Madrid, Spain, in 2005. She received the Ph.D. degrees in electrical engineering from the University of Valladolid (UVA), Spain, in 2018. She is currently a Professor with the UEMC. Her current research interests are monitoring of induction machines, detection and diagnosis of faults in inverter-fed IM in transient regimes.

Joan Pons-Llinares (M'13) received the M.Sc. degree in Industrial Engineering and the Ph.D. degree in Electrical Engineering from the Universitat Politècnica de València (UPV, Spain), in 2007 and 2013, respectively. He is currently an Associate Professor in the Electric Engineering Department of the UPV. His research interests include time-frequency transforms, condition monitoring and efficiency estimation of electrical machines.

Oscar Duque-Perez is an associate professor of Electrical Engineering at the University of Valladolid (UVa), Spain. He received his B.S. and Ph.D. from UVa, in 1992 and 2000, respectively. In 1994, he joined the Department of Electrical Engineering of the School of Industrial Engineering, UVa. He is a member of the research group on Analysis and Diagnostics of Electrical Grids and Installations (ADIRE) and ITAP, University of Valadolid. He has published over 100 journal and conference papers and has been collaborating in R+D Projects with Private Companies such as Iberdrola, Adif or Redalsa as well as R+D public funded projects for more than twenty years. Duque-Perez received the Thomas Hawskley Gold Medal from the Institution of Mechanical Engineers, UK and the William Alexander Agnew Meritorious Award/Clarence Noel Goodall Award from the Institution of Mechanical Engineers, Railway Division, UK. His main research fields are electric machines condition monitoring, power systems reliability and power quality, and electric energy efficiency.

D. Morinigo-Sotelo (M'04) received the B.S. and Ph.D. degrees in electrical engineering from the University of Valladolid (UVA), Spain, in 1999 and 2006, respectively. He was a research collaborator on Electromagnetic Processing of Materials with the Light Alloys Division of CIDAUT Foundation since 2000 until 2015. He is currently with the research group on Analysis and Diagnostics of Electrical Grids and Installations (ADIRE), that belongs to the ITAP Institute (UVA), and with the HSPdigital Research Group, Mexico. His current research interests include fault detection and diagnostics of induction machines, power quality, and smart grids.